IOSR Journal of Applied Chemistry (IOSR-JAC)
e-ISSN: 2278-5736.Volume 9, Issue 7 Ver. I (July 2016), PP 06-22
www.iosrjournals.org

Synthesis, characterization, equilibrium studies, DNA binding and anti microbial activity of 2-Propionyl-amino-5- alkyl, 1,3,4-thiadiazoles and their complexes

Firasath Unnisa[a], B. Sireesha[a]*and D. A. Padmavathi[b]
[a]*Department of Chemistry, Nizam College, O.U., Basheerbagh, Hyderabad, India.*
[b]*University College of Science, Saifabad, Hyerabad.*
**berleysiree@gmail.com*

Abstract: *2-propionyl-amino-5-Methyl-1,3,4-thiadiazole (PAMTDA) and 2-propionyl-amino-5-ethyl-1,3,4-thiadiazole (PAETDA) and their Ni(II) and Zn(II) complexes were synthesized and characterized using LC-MS, IR, UV, ESR, ^{1}H-NMR,(D_2O exchangeable),^{13}C-NMR and TGA. The proton-ligand and metal-ligand constants[M=Ni(II), Zn(II)] of these compounds were determined in 70%(v/v) DMF-water medium at 0.1M KNO_3 ionic strength and 303K temperature by using Irving-Rossetti titration method and the stability constant (Log β) values were found to follow Irving William series of stability of complexes. Computational energy calculations (semi-empirical) were performed on geometrically optimized keto and enol forms of the title compound. Minimum energy values, Heats of formation, dipole moments of the optimized geometries are evaluated, electrostatic potential maps and HOMO, LUMO surfaces are generated. The interaction of metal complex with calf thymus DNA (CT DNA) was evaluated and DNA binding studies were carried out using UV absorption spectroscopy, spectrofluorophotometry and viscosity measurements. Anti bacterial activity of diamagnetic Zn(II) complexes were found to be high compared to Ni(II) complexes against gram(+) and gram (-)bacteria.*

Keywords: *Potentiometric titrations, spectrofluorophotometry, thermal analysis, UV absorption spectroscopy, viscosity measurements.*

I. Introduction

2,5-disubstituted 1,3,4-thiadiazole derivatives represents an interesting class of compounds possessing a wide spectrum of biological activities such as insecticidal[1,2], fungicidal[1,2], trypanocidal[1,3], leishmanicidal[1,3], herbicidal[4], plant growth regulators[4,5] and pharmacological activities[6,7,8] as well as an excellent metal ion coordinating property. They possess a unique role in self organization of potential metal organic complexes through coordination to different transition metal ions. They are also an important organic reaction intermediates and analytical reagents[9,10]. Substituted 1,3,4-thiadiazoles have become very useful compounds in many fields of technology such as lubricating,[10,11,12] composition optically active liquid crystals[10], photographic materials, agrochemicals and dyes[10] and anti corrosive agents [13,14].

1,3,4-thiadiazole ring and its derivatives possess good coordination behaviour since they have sulphur and nitrogen atom in addition to the substituents having a donating group in the structure and probably due to strong aromaticity of the ring system[15]. The complexes of thiadiazoles have received considerable attention for the past few years due to their specific structures, characteristics and reactivity as well as their special biological activities and potential industrial applications [16].

The present work involves the synthesis of 2-propionyl-amino-5-methyl-1,3,4-thiadiazole (PAMTDA) and 2-propionyl-amino-5-ethyl-1,3,4-thiadiazole (PAETDA) from reported procedure and their metal complexes using metal chlorides [M= Ni(II) and Zn(II)], their characterization, equilibrium studies, DNA binding studies and anti microbial studies.

II. Experimental

2.1. Materials and Methods:

All the chemicals and solvents used were of AnalaR grade and used without further purification. All metal salts were used as chlorides. Thin layer chromatography was used to access the reactions and purity of compounds synthesized. Melting points were recorded on a Toshniwal hot stage apparatus in open capillary tubes and presented uncorrected. LC-MS of ligands and their complexes were recorded on LC-MS 2010A Shimazdu spectrometer. IR was recorded on Shimazdu Prestige-21 FTIR spectrophotometer in KBr disc. UV spectra were obtained in DMSO solution from Shimazdu UV 2450 spectrophotometer within the range of 200-1000nm. ^{1}H-NMR (with D_2O exchange) and ^{13}C-NMR spectra were recorded on Bruker WH-270MHz using TMS as internal standard and chemical shift in δppm. Thermogravimetric analyses were carried out on Perkin-

Elmer model TGS-2. Conductance of the metal complexes was measured in DMSO on a Digisun digital conductivity meter model D1 909 at room temperature. Magnetic measurements were made on solid complexes using Guoy method on Faraday balance model 7550. The proton ligand and metal ligand formation constants for complexes were determined potentiometrically using Irving Rossetti titration technique, and the pH measurements were made using a digital Elico Electronic model LI-120 pH meter in conjunction with a combined glass and calomel electrode. Semi-empirical AM1, quantum chemical calculations were carried out by the HyperChem^{TM} 7.5 Molecular Modeling program. DNA binding studies were carried out using U.V absorption spectroscopy, emission spectral study was carried out using Shimazdu RF 5301 PC spectrofluorophotometer and Viscosity measurements were carried out using an Ostwald's viscometer maintained at a constant temperature of 30.0±0.1 °C in a thermostatic water-bath. Antimicrobial activity was tested using Disc Diffusion method.

2.2. Synthesis of 2- propionyl-amino-5-methyl-1,3,4-thiadiazole(PAMTDA):

Synthesis of 2-propionyl amino-5-methyl-1,3,4-thiadiazole (PAMTDA) involves two steps.

2.2.1. Step-I: Synthesis of 2-amino-5-methyl-1,3,4-thiadiazole: 2-amino-5-methyl-1,3,4-thiadiazole was prepared[17,18] by refluxing 0.022M of thiosemicarbazide with 0.02M of acetic acid in presence of Conc. H_2SO_4 for 6 hours and then neutralizing with ammonia solution or 1M Na_2CO_3 solution under cool condition. The compound obtained was filtered, dried and recrystallized using ethanol. The purity of the compound was checked using TLC. The melting point of compound was found to be 220°-222°C.

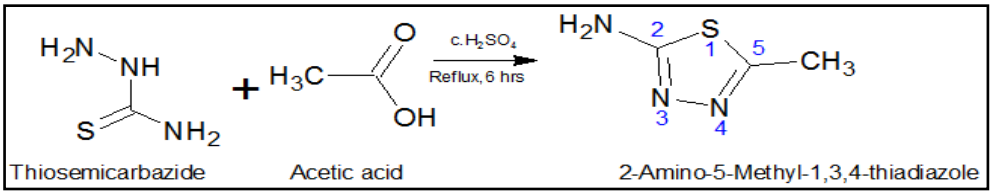

Scheme1a: Synthesis of 2-amino-5-methyl-1,3,4-thiadiazole

2.2.2. Step-II: Synthesis of 2-propionyl-amino-5-methyl-1,3,4-thiadiazole: 2-propionyl-amino-5-methyl-1,3,4-thiadiazole was prepared[19,20] by refluxing 2gm (0.017M) of 2-amino-5-methyl-1,3,4-thiadiazole with 2ml (0.02M) of propionyl chloride under anhydrous conditions for 3hrs. The compound obtained was washed repeatedly with ice cold water to remove excess of propionyl chloride. The compound was recrystallized using 60% ethanol. The purity of compound was checked using TLC. The melting point of the compound was found to be 266°-268°C.

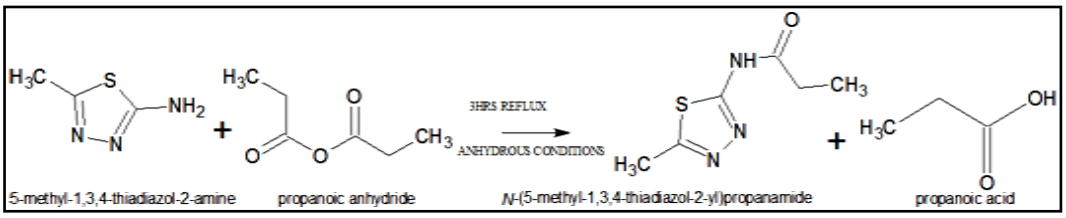

Scheme1b: Synthesis of 2-propionyl-amino-5-methyl-1,3,4-thiadiazole (PAMTDA)

2.3. Synthesis of 2-propionyl-amino-5-ethyl-1,3,4-thiadiazole(PAETDA): 2-propionyl-amino-5-ethyl-1,3,4-thiadiazole (PAETDA) was prepared[21] by refluxing 3gm (0.032M) of thiosemicarbazide with 9.065ml (0.098M) of propionyl chloride under anhydrous conditions for 3 hrs. The white solid obtained in the refluxing flask was washed repeatedly with ice cold water to remove excess of propionyl chloride. The compound obtained was dried and recrystallized using 60% ethanol solution. The purity of the compound was checked by TLC. The melting point of the compound was found to be 218°C -222°C.

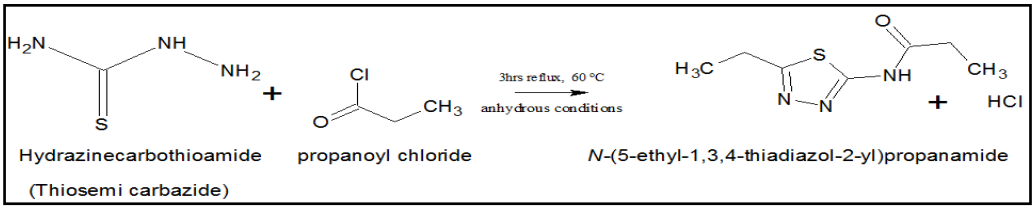

Scheme2: Synthesis of 2- Propionyl-amino-5-ethyl-1,3,4-Thiadiazole(PAETDA)

2.4. Preparation of metal complexes:

Ni(II) and Zn(II) complexes of PAMTDA and PAETDA were prepared by refluxing the metal salt solutions of Zinc chloride (0.015M) and Nickel chloride(0.015M) with hot methanolic solution of PAMTDA (0.03M) and Zinc chloride (0.0014M) and Nickel chloride(0.0014M) with hot methanolic solution of PAETDA (0.028M), that is in 1:2 molar ratio for 15-20hrs. pH was adjusted with methanolic ammonical buffer (pH≈8). Solid complexes separated were washed with hot methanol to remove unreacted ligand then with double distilled water to remove unreacted metal salt and finally with petroleum ether. The solid complexes obtained were dried over fused $CaCl_2$, in a vacuum desiccators at room temperature.

2.5 Computational studies

Keto and enol forms of PAMTDA and PAETDA were built, their geometry optimization was performed and the orbital energy diagrams are generated using HyperChem™ 7.5. The total energy, heat of formation and dipole moment of the optimized geometries are calculated. Electrostatic potential diagrams are mapped. Highest occupied molecular orbital (HOMO), Lowest unoccupied molecular orbital (LUMO) have been generated. Important physical parameters like energies of HOMO and LUMO, their gap, hardness(η), ionization potential(IP), and electron affinity(EA) that are important for studying chemical reactivity and biological properties are calculated [22,23]. Electrostatic potential mapping, reveal the reactive sites on the molecules [24,25].

III. Results and Discussion

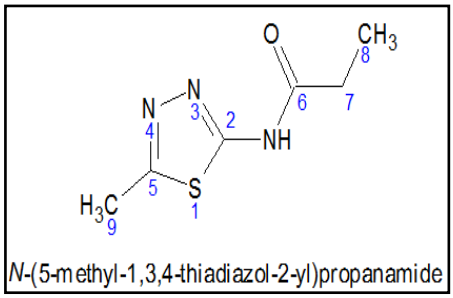

1(a): PAMTDA

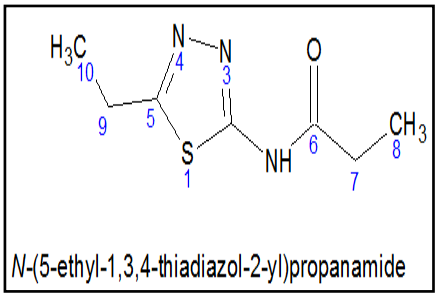

1(b): PAETDA

Fig. 1(a&b): Structures of PAMTDA and PAETDA

3.1. Characterization of ligands:

3.1.1. LC-MS: The liquid chromatogram of PAMTDA showed a single peak with retention time of 0.588min., indicating the purity of compound. The ESI(-ve) mass spectrum of PAMTDA (Fig.2a) showed following peaks, a peak at m/z170 $(M-1)^{+\cdot}$, m/z173 $(M+2)^{+\cdot}$, m/z156 $(M-CH_3)^{+\cdot}$, m/z142 $(M-C_2H_5)^{+\cdot}$, m/z114 $(M-COC_2H_5)^{+\cdot}$, m/z342 (dimer).

The liquid chromatogram of PAETDA showed a single peak with retention time of 0.657min. reveal its purity. The APCI(+) mass spectrum of PAETDA (Fig.2b) showed base peak at m/z 186 $(M+1)^{+\cdot}$, 187 $(M+2)^{+\cdot}$ molecular ion peaks, m/z 130 $(C_4N_3SH_6)^{+\cdot}$ and m/z 115$(C_4N_2SH_5)^{+\cdot}$.

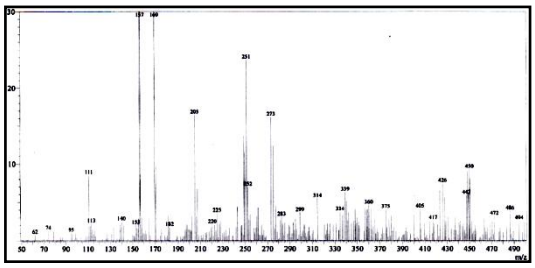

2(a): PAMTDA

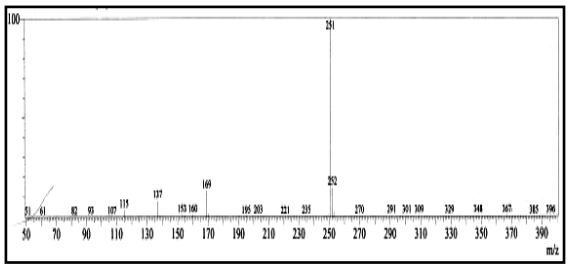

2(b): PAETDA

Fig.2(a&b): Mass spectra of ligands

3.1.2. IR spectrum: IR spectrum of PAMTDA (Fig.3a) showed the characteristic bands at 3165cm^{-1} $\upsilon_{(2^{o}N-H)}$, 2977-2912cm^{-1} $\upsilon_{(C-H)}$, 1689cm^{-1} $\upsilon_{(C=O)}$, 1573cm^{-1} $\upsilon_{(O=C-NH)}$, 1567cm^{-1} thiadiazolic ring $\upsilon_{(C=N-3)}$, 1450cm^{-1} $\upsilon_{(C=N-4)}$, 1418cm^{-1} $\upsilon_{(C-N-S)}$, 1300cm^{-1} $\upsilon_{(N=C-N)}$, 1256cm^{-1} $\upsilon_{(N-C=O)}$, 1207cm^{-1} $\upsilon_{(C-C)}$, 1067cm^{-1} $\upsilon_{(N-N)}$, 830cm^{-1} $\upsilon_{(C5-S)}$ and 706cm^{-1} $\upsilon_{(C2-S)}$ [27].

IR spectrum of PAETDA(Fig.3b) showed the stretching frequency bands at 3186cm^{-1} $\upsilon_{(2^{o}N-H)}$, 2745-2980cm^{-1} $\upsilon_{(C-H)}$,1690cm^{-1} $\upsilon_{(C=O)}$, 1573cm^{-1} $\upsilon_{(O=C-NH)}$, 1566cm^{-1} thiadiazolic ring $\upsilon_{(C=N-3)}$,1495cm^{-1} $\upsilon_{(C=N-4)}$, 1300cm^{-1} $\upsilon_{(N=C-N)}$, 1248cm^{-1} υ $_{(N-C=O)}$, 1194cm^{-1} $\upsilon_{(C-C)}$,1046cm^{-1} υ $_{(N-N)}$, 835cm^{-1} $\upsilon_{(C5-S)}$ and 704cm^{-1} $\upsilon_{(C-S)}$ [27].

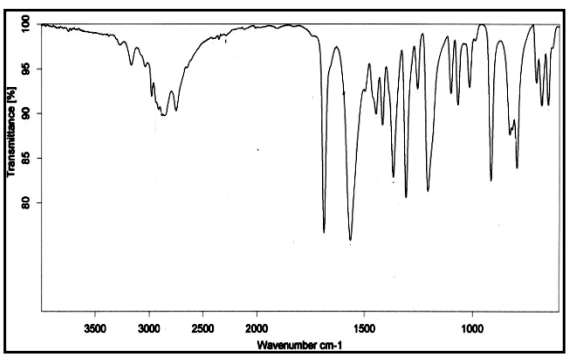

3(a): PAMTDA

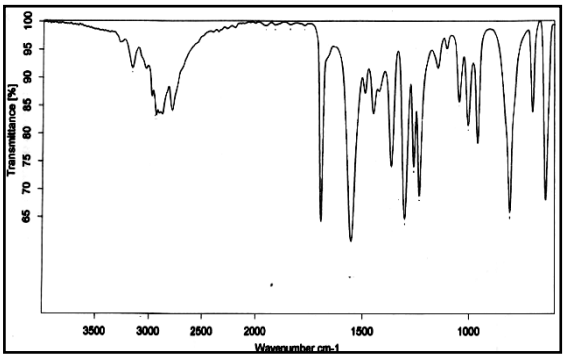

3(b): PAETDA

Fig.3 (a&b): IR spectra of ligands

3.1.3. ^{1}H-NMR: ^{1}H-NMR spectrum [28] of PAMTDA (Fig.4a) in DMSO d^{6} showed singals at ppm δ1.24 (t, 3H, (C8) CH_3 protons), δ2.5 (s, 3H, (C9) CH_3 protons), δ4.74 (q, 2H (C7) protons), and δ12.8 (s, 1H, NH proton). The chemical shift of amide 2°(NH) proton is supported by the D_2O exchangeable spectrum.

^{1}H-NMR spectrum of PAETDA (Fig.4b) in DMSO d^{6} showed signals at ppm δ1.31 (t, 3H, (C10) CH_3 protons), δ1.42 (t, 3H, (C8) CH_3 protons), δ2.78 (q, 2H (C9) protons), δ3.06 (q, 2H (C7) protons) and δ13.3 (s, 1H, NH proton). The chemical shift of amide 2°(NH) proton is supported by the D_2O exchangeable spectrum.

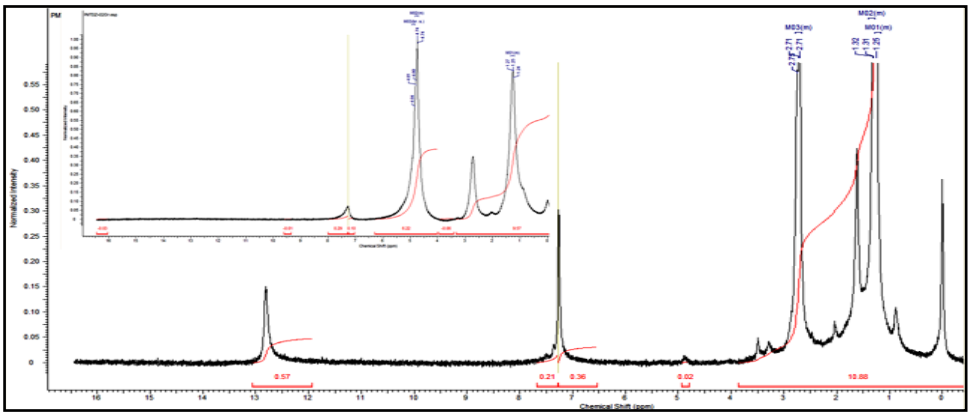

4(a): PAMTDA

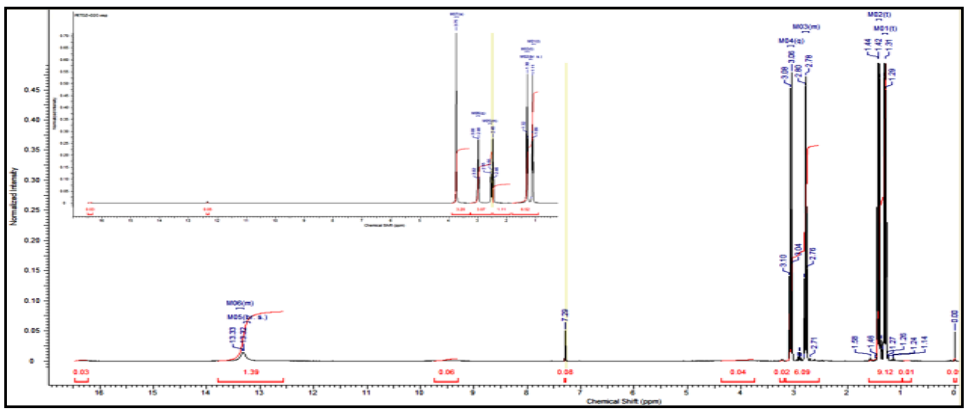

4(b): PAETDA

Fig.4 (a&b): ^{1}H-NMR of ligands with D2O exchangeable

3.1.4. ^{13}C-NMR: ^{13}C-NMR [28] spectrum of PAMTDA (Fig.5a) showed the signals corresponding to 6 carbons in the compound at ppm δ9 (C_8), δ14.67 (C_9), δ28.14 (C_7), δ158.36 (C_5), δ165.12 (C_2) and δ172.02 (C_6).

^{13}C-NMR spectrum of PAETDA (Fig.5b) showed the signals corresponding to 7 carbons in the compound at ppm δ10 (C_{10}), δ18 (C_8), δ24 ppm (C_9), δ30 (C_7), δ160 (C_5), δ168 (C_2) and δ179(C_6).

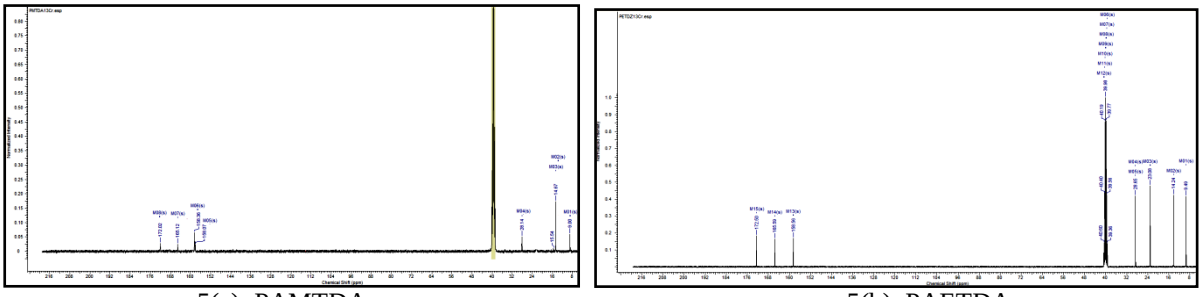

5(a): PAMTDA 5(b): PAETDA

Fig.5 (a&b): ^{13}C-NMR of ligands

3.1.5. UV-Visible spectra: The UV-Visible spectrum of PAMTDA (Fig.6a) showed a highly intense peak at 38910 cm^{-1} corresponding to n→ π^* transition in C=O of amide. The UV-Visible spectrum of PAETDA (Fig.6b) also showed an intense peak at 30674cm^{-1} corresponding to n→ π^* transition in C=O of amide.

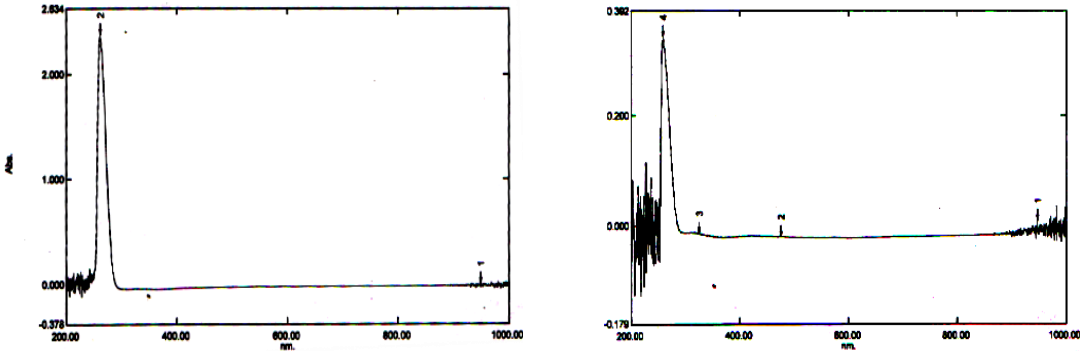

6(a): PAMTDA 6(b): PAETDA

Fig.6 (a&b): UV-Visible spectra of the compounds

3.1.6: Equilibrium studies: The determination of acid dissociation constant of the compounds PAMTDA and PAETDA and the stability constants of their metal complexes with Ni(II) and Zn(II) were carried out by using potentiometric Irving-Rossetti titration method [29,30] at 30^{o}C and ionic strength of 0.1M (KNO_3) in 70% v/v DMF-water medium. The dissociation constants of PAMTDA and PAETDA and their stability constants with Ni(II) and Zn(II) ions were calculated. Both the ligands were found to be monobasic acids, with one dissociable proton, corresponding to amide nitrogen in the keto form of ligand or from hydroxyl group in the enol form (Fig.7).

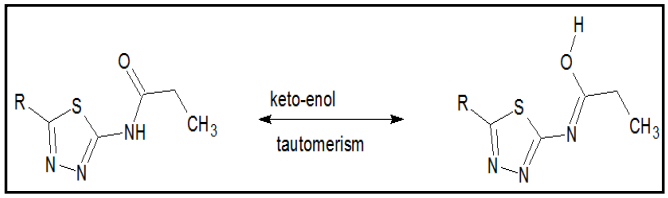

Fig.7: Keto-enol tautomerism

The dissociation constant values of these ligands are found to be: 9.98 for PAMTDA and 10.04 for PAETDA. The high value of pK_a for PAETDA is due to the presence of ethyl group at fifth position, where as in PAMTDA methyl group is present at fifth position. As methyl group is less electron donating than ethyl, the proton gets dissociated easily in case of PAMTDA, hence more acidic and show low pK_a value than PAETDA.

The stability constant values of Ni(II) and Zn(II) complexes were obtained from the plot of Log 1- $\bar{n}$ / n vs pL for 1:1 M-L complex and Log 2- $\bar{n}$ / n -1 vs pL for 1:2 M-L complex (Fig. 8a-e). The stability constant values (Log β) for all the complexes Log β_2 obtained for Ni(II)-PAETDA binary system are presented in Table 1.. Thus from equilibrium studies the composition of Ni(II)-PAETDA complex is found to be1:2,, whereas the composition of other complexes is 1:1. The stability of the Ni(II) and Zn(II) complexes follows the Irving William series of stability of complexes with both the ligands i.e. Zn(II) >Ni(II).

$\bar{n}$	Log $(1-\bar{n})/\bar{n}$	pL
0.6926	-0.35	5.98
0.6325	-0.23	6.09
0.5862	-0.15	6.19
0.5468	-0.08	6.29
0.50	0	6.39
0.4848	0.026	6.48
0.431	0.08	6.56
0.4064	0.16	6.68
0.3732	0.22	6.78
0.3199	0.32	6.89

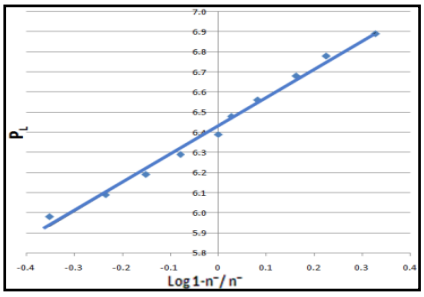

Fig.8(a): pL graph of Zn(II)-PAMTDA

$\bar{n}$	Log $(1-\bar{n})/\bar{n}$	pL
0.6075	-0.25	9.1
0.5925	-0.16	9.2
0.5725	-0.12	9.3
0.547	-0.08	9.4
0.515	-0.04	9.5
0.488	0.03	9.6
0.45	0.083	9.7
0.43	0.12	9.8
0.393	0.18	9.9
0.353	0.26	10.05

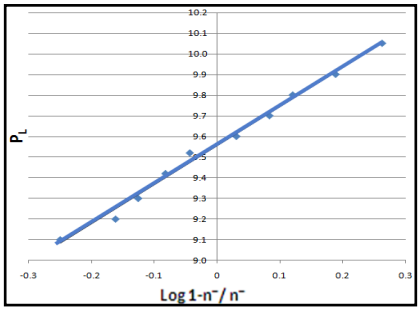

Fig.8 (b)**:** pL graph of Zn(II)-PAETDA

$\bar{n}$	Log $(1-\bar{n})/\bar{n}$	pL
0.7287	-0.42	5.91
0.6997	-0.36	6.01
0.6145	-0.20	6.14
0.5534	-0.09	6.24
0.5064	-0.011	6.34
0.4817	0.03	6.41
0.426	0.13	6.51
0.3689	0.23	6.61
0.3231	0.32	6.71
0.2964	0.37	6.81

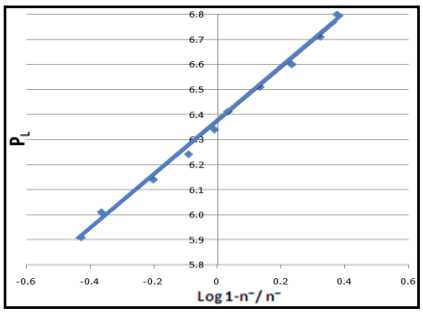

Fig.8(c): pL graph of Ni(II)- PAMTDA

$\bar{n}$	Log $(1-\bar{n})/\bar{n}$	pL	$\bar{n}$	Log $(2-\bar{n})/(\bar{n}-1)$	pL
0.6128	-0.19	8.44	1.92	-1.06	3.4
0.575	-0.13	8.55	1.87	-0.82	3.5
0.5638	-0.11	8.66	1.79	-0.57	3.6
0.5444	-0.077	8.76	1.68	-0.32	3.7
0.5233	-0.04	8.86	1.5	0	3.8
0.4816	0.03	9.04	1.45	0.071	3.9
0.4496	0.087	9.15	1.32	0.32	4.0
0.4377	0.108	9.24	1.22	0.54	4.1
0.416	0.14	9.33	1.1	0.95	4.2
0.392	0.19	9.44	1.07	1.12	4.3

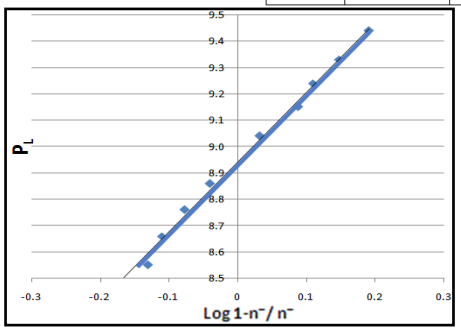

8(d)

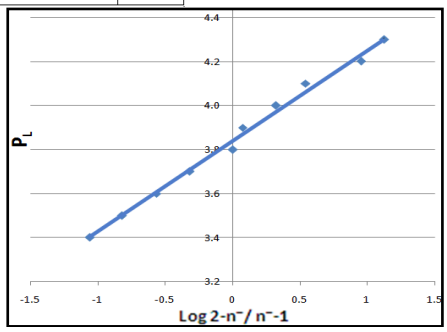

8(e)

Fig 8(d&e): pL graphs of Ni(II)-PAETDA

Table:1 Dissociation constant and stability constant values in 70% v/v DMF- water medium at temperature 30^{o}C and 0.1M(KNO_3) ionic strength

Ligand	Metal(II) ion	Log K_1	Log K_2	Log β
PAETDA	Zn(II)	9.565	-	9.565
(pKa-10.04)	Ni(II)	8.493	3.84	12.33
PAMTDA	Zn(II)	6.432	-	6.432
(pKa-9.98)	Ni(II)	6.367	-	6.367

3.2 Computational study of PAMTDA and PAETDA

To understand the stability and reactivity of PAMTDA and PAETDA, semi-empirical AM1 calculations have been carried out. Keto and enol forms of the compounds were built, pre-optimized with molecular mechanics (AMBER) and then optimized more accurately with AM1 semi-empirical calculations. Single point energy, heat of formation and dipole moment of the optimized geometries were calculated using quantum mechanics and are presented in Table 2.

Table: 2 Molecular Properties of PAMTDA and PAETDA

Molecular Properties	PAMTDA		PAETDA	
	Keto	Enol	Keto	Enol
Single Point Energy (kcal/mol)	-1925.21	-1893.95	-2208.06	-2198.44
Heat of formation (kcal/mol)	34.46	37.23	44.40	29.02
Dipole Moment (Debye)	6.16	4.14	6.12	3.72

The lower energies indicate that both keto and enol forms of the compounds are stable. Close proximity in energies of keto and enol forms indicate the possibility of co-existence of both the forms. Calculated dipole moment values indicate more polar nature.

3.2.1. FMO Analysis: Analysis of HOMO and LUMO of the chemical compounds play an important role in understanding its chemical reactivity. Ionization energy (IE), electron affinity (EA) and hardness can be expressed as – E_{HOMO} – E_{LUMO} and 1/2(E_{HOMO}- E_{LUMO}) respectively [24,25] and are shown in Table 3. A system with large gap between HOMO and LUMO will be less reactive and is harder in nature. In the present study, this gap is between 7.584 and 8.644eV indicating the stability and hardness of the molecule in all the two forms of the compounds also supported by their ionization energy.

Table: 3 Comparison of HOMO–LUMO energy, hardness, ionization energy, electron affinity

	PAMTDA		PAETDA	
Energies	Keto	Enol	Keto	Enol
E_{HOMO} (ev)	-9.295	-8.8145	-9.296	-9.271
E_{LUMO} (ev)	-0.651	-1.230	-0.693	-0.844
E_{HOMO}- E_{LUMO} (ev)	8.644	7.584	8.597	8.426
Hardness=1/2 (E_{HOMO}- E_{LUMO})	4.756	3.790	4.290	4.213
I.E=- E_{HOMO}	9.300	8.814	9.296	9.270
EA=- E_{LUMO}	0.651	1.230	0.693	0.843

The optimized structures of Keto and enol forms of both the compounds, electrostatic potential, and the generated molecular orbital energy diagrams, HOMO and LUMO are presented in Fig: 9 and 10. Electrostatic potential mapping gives information about the reactivity of the molecule with nucleophilic/electrophilic reagents. From the electrostatic potential mapping violet region around oxygen, and nitrogen atoms with amide and azomethine linkage(keto and enol form) respectively and nitrogens of thiadiazole ring indicate negative ESP, hence more susceptible to electrophilic attack by a suitable molecule.

Fig 9: Tautomers of PAMTDA

Keto form of PAMTDA Enol form of PAMTDA

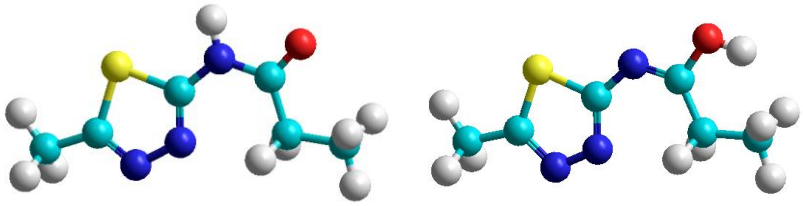

Fig 9a. Optimized geometry of PAMTDA

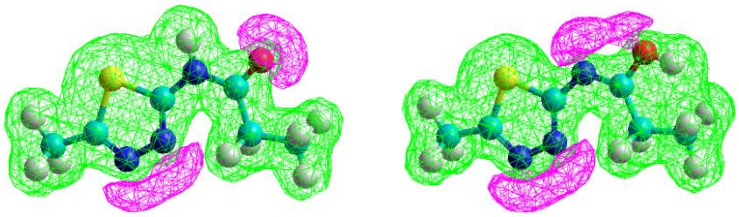

Fig 9b. Electrostatic potential mapping of of PAMTDA

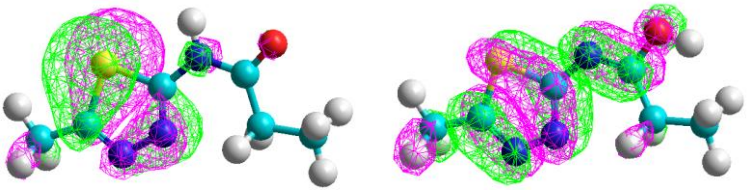

Fig 9c. Highest occupied molecular orbitals of PAMTDA

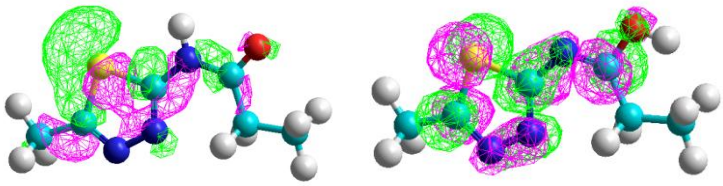

Fig 9d. Lowest unoccupied molecular orbitals of PAMTDA

Fig 10: Tautomers of PAETDA

Keto form of PAETDA Enol form of PAETDA

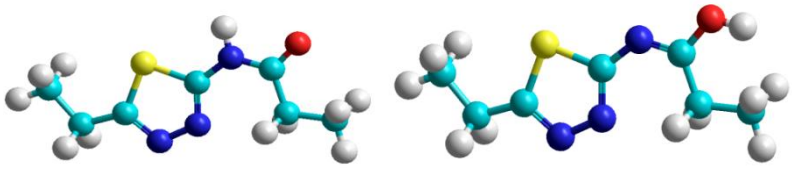

Fig 10a. Optimized geometry of PAETDA

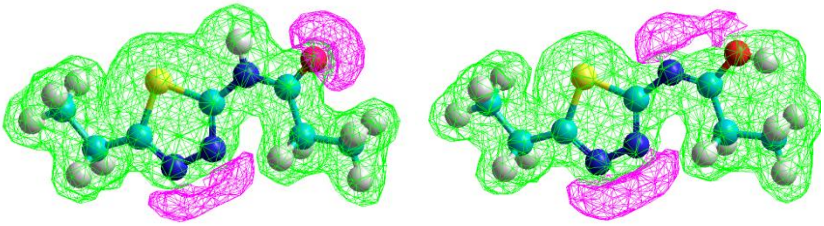

Fig 10b. Electrostatic potential mapping of PAETDA

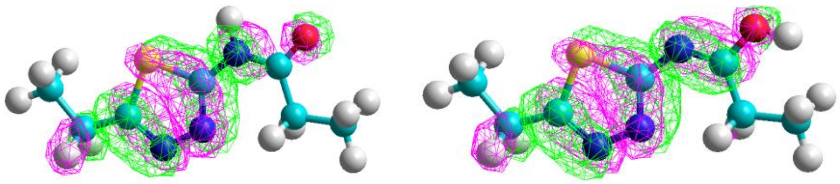

Fig 10c. Highest occupied molecular orbitals of PAETDA

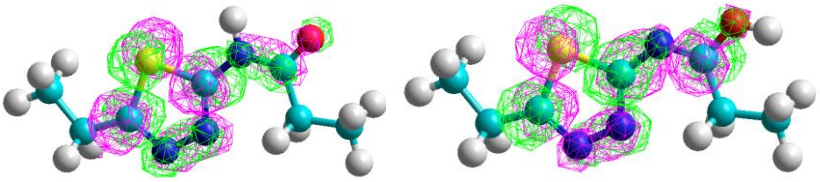

Fig 10d. Lowest unoccupied molecular orbitals of PAETDA

3.2.2. QSAR Studies: QSAR studies helps to recognize and compute the physico-chemical properties of a drug and its effect on biological activity. The most common physic-chemical properties include hydrophilic, electronic and steric nature. Hydrophobic character of a drug is crucial in identifying its ease in crossing the cell membrane and its interaction with the receptor. It is measured in terms of partition coefficient.

Partition coefficient = Conc. of drug in octanol / Conc. of drug in aqueous solution (1)

By plotting log p vs log 1/concentration, it is possible to correlate drug with biological activity. In general, drugs with log p nearly 3.0 have greater chance of being absorbed, higher than 4.0 require lipid formulations and less than 2.0 shows both hydrophilic and hydrophobic character and are difficult to formulate. From log p values of the ligand (Table: 4) in keto and enol forms it can be understood that ligand possess good penetrating capability into cell membrane and in turn has considerable biological activity [26].

Table: 4 QSAR properties of PAETDA and PAETDA

Properties (AM1)	PAMTDA		PAETDA	
	Keto	Enol	Keto	Enol
Partial charge	0.00e	0.00e	0.00e	0.00e
Surface area (approx) (Å^2)	362.30	340.79	391.69	374.56
Surface area (grid) (Å^2)	361.12	361.49	394.84	395.18
Volume (Å^3)	543.10	544.64	596.06	596.98
Hydration energy (K.cal/mol)	-9.66	-11.67	-8.65	-10.99
Log P	1.35	2.35	1.97	2.97
Refractivity (Å^3)	43.91	44.14	48.54	48.77
Polarizability (Å^3)	17.32	17.45	19.15	19.18
Mass (amu)	171.22	171.22	185.24	184.24

3.3: Characterization of metal complexes

3.3.1: Physical properties: Zn(II)-PAETDA and Zn(II)- PAMTDA complexes are white amorphous solids whereas Ni(II)-PAETDA and Ni(II)-PAMTDA complexes are light green and bluish green in colour respectively. All the complexes are sparingly soluble in DMF and DMSO, stable at room temperature but on heating above 300°C undergoes decomposition. Volhardt's test [31] indicate the presence of chloride ion outside the coordination sphere in Zn(II)-PAETDA, inside the coordination sphere in Ni(II)-PAMTDA and Zn(II)-PAMTDA whereas Ni(II)-PAETDA showed negative result.

3.3.2: LC-MS: The liquid chromatogram of Zn(II)-PAMTDA showed a single peak with retention time of 0.559min indicating the purity of compound. ESI(+) mass spectrum of complex (Fig.11a) showed a peak at m/z345 (343.38) corresponding to $[Zn(C_6H_9N_3OS)2H_2O.2Cl]^{+\cdot}$, m/z272 (271.38) due to $[Zn(C_6H_9N_3OS)\ 2H_2O]^{+\cdot}$, m/z255 (254.38) due to $[\ Zn(C_6H_9N_3OS)\ H_2O]^{+\cdot}$, m/z237 (236.38) $Zn(C_6H_9N_3OS)^{+\cdot}$ indicating 1:1 [M:L] ratio of the complex .

The liquid chromatogram of Zn(II)-PAETDA showed a single peak with retention time of 0.638min indicating the purity of compound. The APCI(+) mass spectrum of Zn-PAETDA (Fig.11b) showed a peak at m/z 358(357.8) is attributed to the molecular ion species $[Zn(C_7H_{10}N_3OS)\ 4H_2O]^{+\cdot}$ Cl, a peak at m/z 325 (323.3) due to metal complex species $[Zn(C_7H_{10}N_3OS)\cdot 4H_2O]^{+\cdot}$, a peak at m/z 305(304.3) is due to complex species$[Zn(C_7H_{10}N_3OS)3H_2O]^{+\cdot}$, a peak at m/z288 (286.3) for species $[Zn(C_7H_{10}N_3OS)\ 2H_2O]^{+\cdot}$, m/z 270

(268.3) $[Zn(C_7H_{10}N_3OS)H_2O]^{+\cdot}$, m/z250 (250.3) is due to complex species $Zn(C_7H_{10}N_3OS)^{+\cdot}$, m/z252 $(M+1)^{+\cdot}$, m/z253 $(M+2)^{+\cdot}$.

The liquid chromatogram of Ni(II)-PAMTDA showed a single peak with retention time of 0.649min indicating the purity of compound. ESI(-ve) mass spectrum of complex (Fig.11c) showed peaks at m/z 370(370.5) $[Ni(C_6H_8N_3OS)Cl\ 3H_2O]^{+\cdot}\ 3H_2O$, m/z 335(336.5) $[Ni(C_6H_8N_3OS)\ 3H_2O]^{+\cdot}3H_2O$, m/z 281 (282.5) $[Ni(C_6H_9N_3OS)\ 3H_2O]^{+\cdot}$, and m/z 226(228) is $Ni(C_6H_9N_3OS)^{+\cdot}$.

The liquid chromatogram of Ni(II)-PAETDA showed a single peak with retention time of 0.551min indicating the purity of compound. The ESI(+) (Fig.11d) mass spectrum of Ni- PAETDA(Fig.9d) showed a peak at m/z516 (515.7) attributed to the molecular ion species $[Ni(C_7H_{10}N_3OS)_22H2O]^{+\cdot}4H_2O$, a peak at m/z479 (478.8) $[Ni(C_7H_{10}N_3OS)_22H_2O]^{+\cdot}H_2O$, m/z461 (461.7) $[Ni(C_7H_{10}N_3OS)_22H_2O]^{+\cdot}$, m/z426 (425.7) $Ni(C_7H_{10}N_3OS)_2^{+\cdot}$, m/z244 (243.7) $Ni(C_7H_{10}N_3OS)^{+}$.

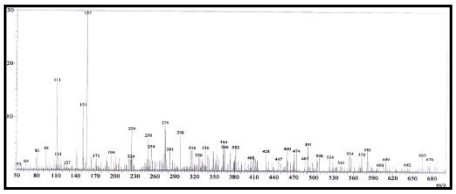

11(a): Zn(II)-PAMTDA

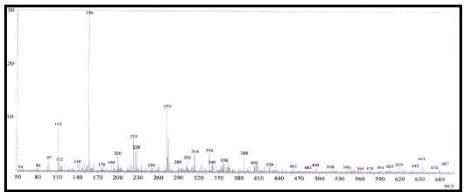

11(b): Zn(II)-PAETDA

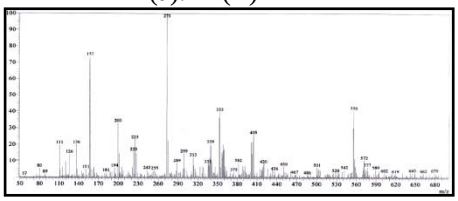

11(c): Ni(II)-PAMTDA

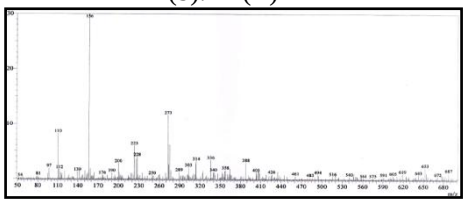

11(d): Ni(II)-PAETDA

Fig. 11(a, b, c & d): Mass spectra of metal complexes

3.3.3: IR SPECTRA: IR spectrum of $[Zn\text{-}(C_6H_9N_3OS\ 2Cl.2H_2O]$ complex (Fig.12a) showed a broad peak at 3200–3400 cm^{-1} indicating the presence of coordinated water, bands at 3227cm^{-1} due to $\upsilon_{(2^{o}N\ -\ H),}$ and 1689cm^{-1} $\upsilon_{(C=O)}$ are observed, thus indicating that the ligand is involved in binding with metal ion in its keto form. A band at 1550cm^{-1} due to $\upsilon_{(C=N-3)}$ of thiadiazole ring is observed at frequency 25 cm^{-1} lower than in ligand PAMTDA IR spectrum due to its involvement in binding with metal ion along with Carbonyl Oxygen, bands at 542cm^{-1} $\upsilon_{(Zn-N)}$[32], 393cm^{-1} $\upsilon_{(Zn-O)}$[32] and 289-300cm^{-1} $\upsilon_{(Zn-H2O)}$ are also observed.

IR spectrum of $[Zn\text{-}(C_7H_{10}N_3OS).4H_2O]$ (Fig.12b) showed a broad peak at 3300-3500cm^{-1} due to presence of coordinated water. Peaks at 3186cm^{-1} $\upsilon_{(2^{o}N\ -\ H)}$ and 1690cm^{-1} $\upsilon_{(C=O)}$ which are present in ligand PAETDA are absent, a new band at 1620cm^{-1} $\upsilon_{(O\text{-}C=N)}$ is seen as a result of enolization of carbonyl group, a band at 1525cm^{-1} $\upsilon_{(C=N-3)}$ of thiadiazole ring is seen at frequency 30-40cm^{-1} lower than in ligand IR spectrum due to its involvement in binding with metal ion along with enolic Oxygen, peaks corresponding to1022cm^{-1} $\upsilon_{(C\text{-}O),}$ 543cm^{-1} $\upsilon_{(Zn-N),}$ 450 cm^{-1} $\upsilon_{(Zn-O),}$ and 394cm^{-1} $\upsilon_{(Zn-H2O)}$ are also present.

IR spectrum of $[Ni(C_6H_8N_3OS)Cl.6H_2O]$ (Fig.12c) showed a broad peak at 3400-3500cm^{-1} due to the presence of coordinated water molecules. Bands corresponding to $\upsilon_{(2^{o}N\text{-}H)}$ and $\upsilon_{(C=O)}$ at 3100cm^{-1} and 1690 cm^{-1} respectively which are present in ligand PAMTDA are absent. A band due to azomethine group $\upsilon_{(O\text{-}C=N)}$ is seen at 1630cm^{-1}, formed as a result of enolization of carbonyl group. A band due to $\upsilon_{(\ C=N-3)}$ of thiadiazole ring is seen at much lower frequency at 1475cm^{-1} due to its involvement in binding with metal ion along with Oxygen of enolic group. Bands at 1062cm^{-1} $\upsilon_{(C\text{-}O),}$ 472cm^{-1} $\upsilon_{(Ni-N),}$ 385cm^{-1} $\upsilon_{(Ni-O),}$ and 280cm^{-1} $\upsilon_{(Ni-H2O)}$ are also observed.

IR spectrum of $[Ni(C_7H_{10}N_3OS)_26H_2O]$(Fig.12d) showed a broad peak at 3300-3500cm^{-1} due to the presence of coordinated water molecules. Bands corresponding to $\upsilon_{(2^{o}N\text{-}H)}$ and $\upsilon_{(C=O)}$at 3100cm^{-1} and 1690cm^{-1} respectively which are present in ligand PAETDA are absent. A band due to azomethine group $\upsilon_{(O\text{-}C=N)}$ is seen at 1633cm^{-1}, formed as a result of enolization of carbonyl group. A band due to $\upsilon_{(C=N-3)}$ of thiadiazole ring is seen at much lower frequency at 1480 cm^{-1} due to its involvement in binding with metal ion along with Oxygen of enolic group. Peaks corresponding to 1065cm^{-1} $\upsilon_{(C\text{-}O),}$ 487cm^{-1} $\upsilon_{(Ni-N)}$ [25], 376cm^{-1} $\upsilon_{(Ni-O)}$ [27], and 275cm^{-1} $\upsilon_{(Ni\text{-}H2O)}$ are also observed.

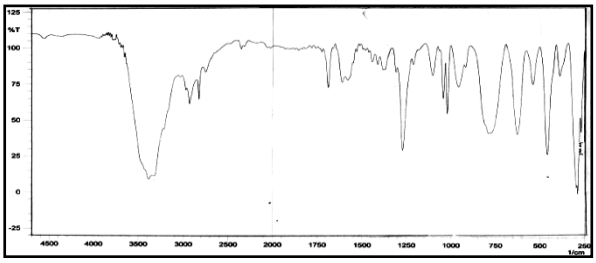

12(a): Zn(II)-PAMTDA

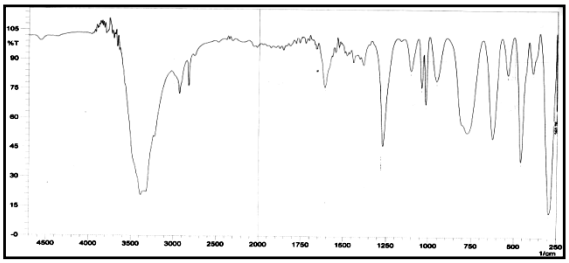

12(b): Zn(II)-PAETDA

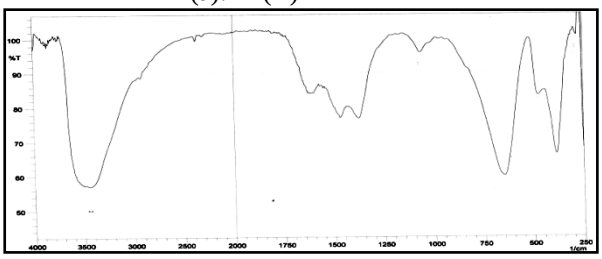

12(c): Ni(II)-PAMTDA

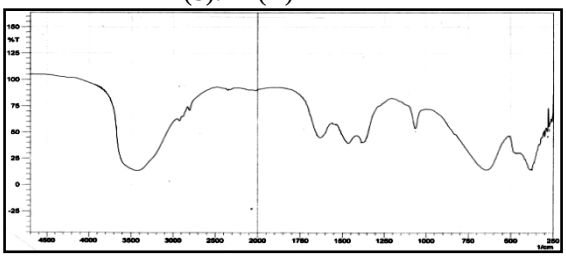

12(d): Ni(II)-PAETDA

Fig.12(a,b,c&d): IR Spectra of metal complexes

3.3.4: ^{1}H-NMR spectrum: The ^{1}H-NMR spectrum of Zn(II)-PAETDA (Fig.13) showed the absence of peak corresponding to the 2^{o}amide (NH) group at δ13.3. Thus indicating the loss of proton while complex formation.

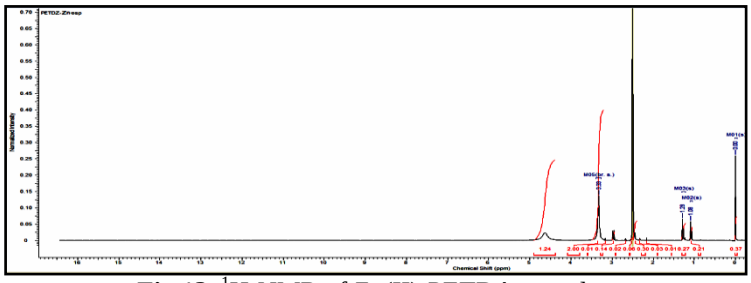

Fig.13: ^{1}H-NMR of Zn(II)-PETDA complex

3.3.5: Thermogravimetric analysis: Thermogram [33] of Zn(II)-PAMTDA (Fig.14a) showed the decomposition of complex in four steps. In first step, the weight loss of 4.418%(15.5g) upto120^{o}C is attributed to the loss of one mole of lattice water. In second step, from 120^{o}C-180^{o}C the weight loss of 10.8% (38.77g) is observed due to loss of two moles of coordinated water. A sudden weight loss of 31.909% (110.18g) is seen from 190^{o}C-492^{o}C corresponding to the partial decomposition of ligand molecule. From 492^{o}C-998^{o}C the %weight loss is about 3.387%(15g).

Thermogram of Zn(II)-PAETDA (Fig.14b) showed the decomposition of complex in three steps. In first step weight loss of about 1% upto120^{o}C does not corresponds to the loss of lattice water. In second step weight loss of 21.157% (76.16g) is seen from 120^{o}C-252^{o}C corresponding to the loss of four moles of coordinated water. A sudden weight loss of 17.268% (62.164g) from 252^{o}C-668^{o}C is attributed to the decomposition of ligand moiety.

Thermogram of Ni(II)-PAMTDA (Fig.14c) complex showed decomposition of complex in three steps. The % weight loss of about 13.25% (49.29g) upto120^{o}C is attributed to loss of three moles of lattice water, from 120^{o}C-280^{o}C the % weight loss is 13.5% (50.22g) which is due to loss of three moles of coordinated water. From 300^{o}C-1000^{o}C there is gradual decomposition of complex. The % of weight left at 1000^{o}C is 22.4% (83g) which corresponds to the weight of NiO corresponding to 1:1 M-L ratio.

Thermogram of Ni(II)-PAETDA (Fig.14d) showed decomposition of complex in three steps. In first step the % weight loss of about 14.2% (70.66g) up to 110^{o}C is observed indicating the loss of four moles of lattice water. In second step the % weight loss of 7.2%(34.56g) from 120^{o}C-280^{o}C is attributed to loss of two moles of coordinated water. From 280^{o}C-600^{o}C there is about 17% (81.719g) weight loss due to partial decomposition of the ligand molecule.

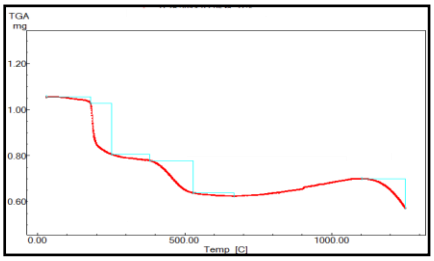

14(a): Zn(II)-PAMTDA

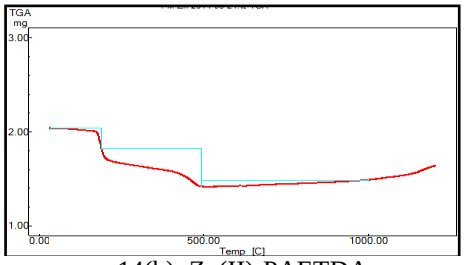

14(b): Zn(II)-PAETDA

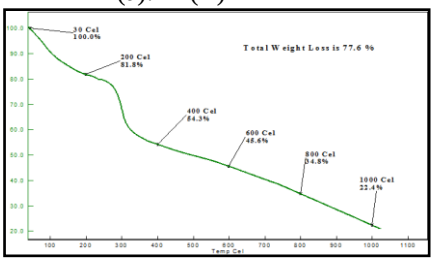

14(c): Ni(II)-PAMTDA

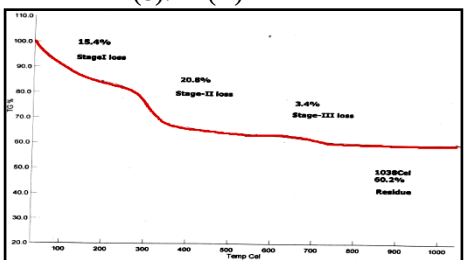

14(d): Ni(II)-PAETDA

Fig.14(a,b,c&d): Thermograms of metal complexes

3.3.6: Magnetic susceptibility: Magnetic moment of Zn(II) complexes were found to be zero due to d^{10} system (diamagnetic). The magnetic moment values of Ni(II)-PAMTDA and Ni(II)-PAETDA were measured to be 2.92BM and 2.84BM respectively, indicating the presence of two unpaired electrons and octahedral geometry [34] around the metal ion.

3.3.7: Electronic spectra [35]**:** The ground state of Ni(II) d^8 system in octahedral geometry is $^3A_{2g}$ (t_{2g}^6 e_g^2) and the Ni(II) complexes of PAMTDA and PAETDA showed the following d-d transitions corresponding to octahedral geometry.

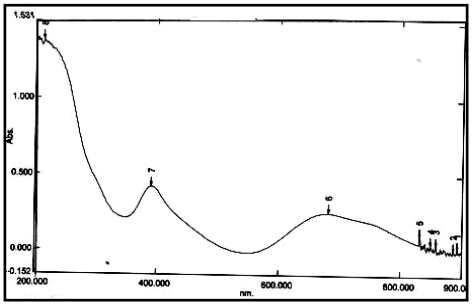

15(a):Ni(II)-PAMTDA

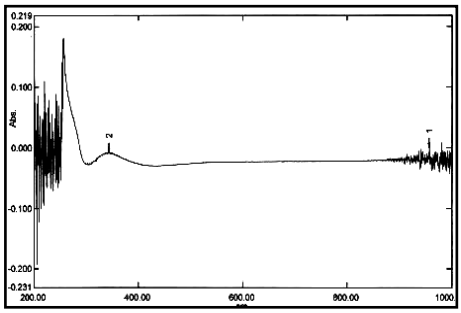

15(b):Ni(II)-PAETDA

Fig.15(a&b): Electronic spectra of Ni(II) complexes

Ni(II)-PAMTDA: The transitions seen in the spectra of the complex are $^3A_{2g}\rightarrow{}^3T_{2g}(F)$ (11,600 cm^{-1}), $^3A_{2g}\rightarrow{}^3T_{1g}(F)$ (12,033 cm^{-1}) and $^3A_{2g}\rightarrow{}^3T_{1g}$ (P) (25,574 cm^{-1}) [31]. A peak at 46,948 cm^{-1} is attributed either to chromophore of ligand or to C-T transition. (Fig.15a).

Ni(II)-PAETDA: It showed peaks due to $^3A_{2g}\rightarrow{}^3T_{2g}(F)$ (10,881 cm^{-1}), $^3A_{2g}\rightarrow{}^3T_{1g}(F)$ (13,175 cm^{-1}) and $^3A_{2g}\rightarrow{}^3T_{1g}(P)$ (32,573 cm^{-1}) transitions [36].(Fig.15b)

3.3.8: Conductivity**:** All the complexes except Zn(II)- PETDA are non–electrolytic in nature due to absence of chloride ion outside the coordination sphere. Zn(II)-PAETDA has shown the conductance of 51$ohm^{-1}cm^2$ mol^{-1} indicating 1:1 electrolytic nature of the complex [37].

3.3.9: Tentative structures of metal-complexes: From the above discussions based on all the analytical, spectral techniques employed and equilibrium studies the following tentative structures for the metal complexes have been proposed. All the complexes were assigned a distorted octahedral geometry. Ni(II)-PAETDA show (1:2) metal-ligand ratio where as all other complexes have (1:1) metal-ligand ratio.

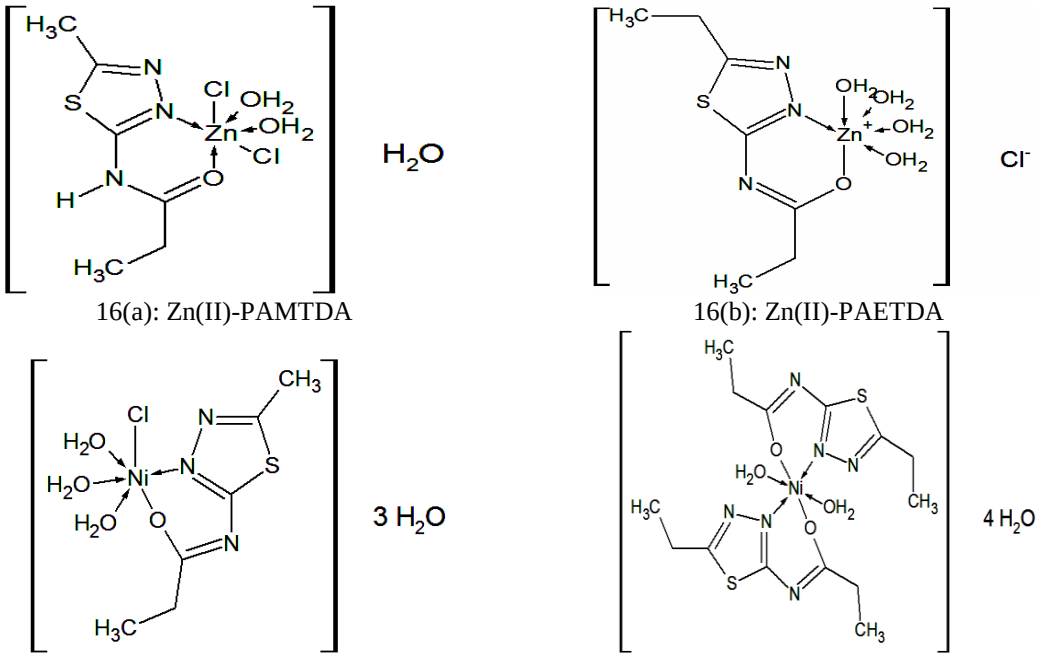

16(a): Zn(II)-PAMTDA 16(b): Zn(II)-PAETDA

16(c): Ni(II)-PAMTDA 16(d): Ni(II)-PAETDA

Fig.16(a, b, c & d): Proposed structures of metal complexes

3.4. DNA binding studies:

3.4. 1. UV-Visible absorption spectroscopy studies: Metal complex titration with calf thymus DNA.

DNA binding experiment was performed in TRIS HCl /NaCl buffer (50mM TRIS HCl /5mM NaCl buffer; pH 7.2), using DMSO solution (10%) of metal complex. The concentration of calf thymus (CT) DNA was determined from the absorption intensity at 260nm with a ε value of $6600M^{-1}cm^{-1}$. Absorption titration experiments were made using different concentrations of CT DNA (20, 40, 60, 80, 100μM) keeping concentration of complex constant [38]. In order to compare quantitatively the binding affinity of complexes with CT-DNA the intrinsic binding constant K_b of the complexes were determined and listed in the Table 5. The non linear least square analysis was performed using Origin pro 6.1.

The binding constant K_b is determined from the spectroscopic titration data using the following equation [33]. $[DNA] / (\varepsilon_a - \varepsilon_f) = [DNA] / (\varepsilon_b - \varepsilon_f) + 1 / Kb(\varepsilon_b - \varepsilon_f)$

Where, $\varepsilon_a = A_{obs} / [complex]$

ε_f and ε_b corresponds to the extinction coefficient for free(unbound) and fully bound complex.

The plot of $[DNA] / (\varepsilon_a - \varepsilon_f)$ vs [DNA] will have a slope equal to $1 / (\varepsilon_a - \varepsilon_f)$ and the intercept equal to $1/Kb(\varepsilon_b - \varepsilon_f)$, K_b is given by the ratio of slope and intercept.

The electronic spectra of the complexes were significantly perturbed by the addition of increasing amounts of CT-DNA. The DNA binding results obtained from electronic spectroscopy suggests that the interaction of the Zn(II)-PAMTDA (Fig. 17a), Zn(II)-PAETDA (Fig. 17b), Ni(II)-PAMTDA(Fig. 17c) and Ni(II)-PAETDA (Fig. 17d) complexes showed hypochromism and bathochromism at 280-300nm (ligand to metal charge transfer band) due intercalation mode of binding with DNA [38,39]. The hypochromism and red shift seen in the absorption spectra is due to strong $\pi \rightarrow \pi^*$ stacking interaction between the aromatic chromophore of the metal complexes and the base pairs of DNA [40].

Table 5: Binding constant Kb of the complexes

Metal complex	Zn-PAMTDA	Zn-PAETDA	Ni-PAMTDA	Ni-PAETDA
Binding constant $(K_b)M^{-1}$	0.173×10^6	0.293×10^6	0.308×10^6	0.497×10^6

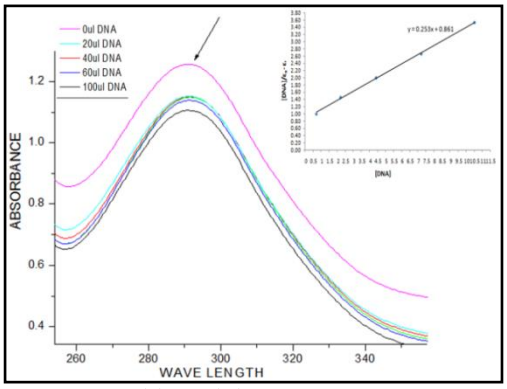

Fig.17(a): Zn(II)-PAMTDA

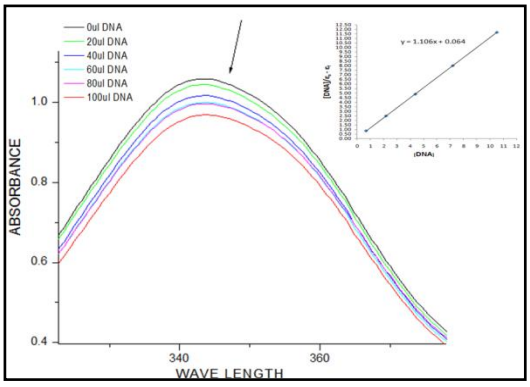

Fig.17(b): Zn(II)-PAETDA

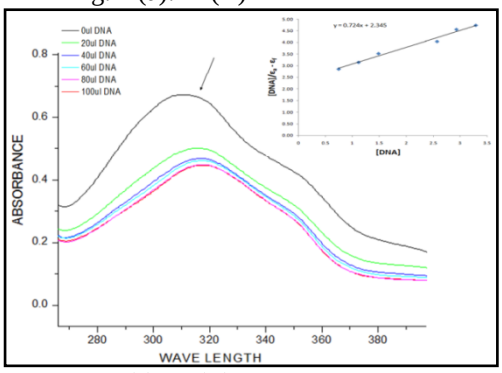

Fig.17(c): Ni(II)-PAMTDA

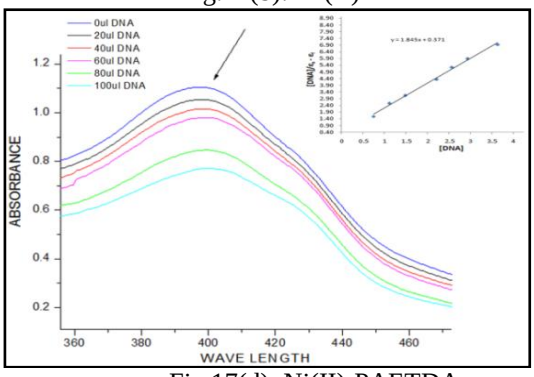

Fig.17(d): Ni(II)-PAETDA

(Insert: plot of [DNA] / (ε_a- ε_f) vs [DNA])

Fig.(17a,17b,17c&17d): Electronic spectra of Zn(II) and Ni(II) complexes showing hypochromic effect and bathochromic shift on increasing the concentration of DNA.

3.4. 2. Fluorescence studies: Competitive binding of metal complex to DNA Ethidium bromide (3,8-diamino-5-ethyl-6-phenyl phenanthridium bromide) is widely used as a sensitive fluorescent probe for DNA due to its high fluorescence when bound to the nucleic acid. When bound to DNA, EtBr shows a remarkable enhancement in fluorescence, due to a steric protection that the nucleobases provide to the dye molecule [41,42]. In the presence of metal-complex having affinity towards DNA may result in a decrease in the emission intensity of the EtBr-DNA adduct, caused by either a competition for binding sites, a change in DNA conformation or through a photoelectron transfer mechanism [43].Thus the affinity of metal complexes towards DNA can be measured by competitive fluorescence studies, as it is a measure of the extent of the emission intensity reduction of the EtBr-DNA adduct.

The quenching of the EtBr-DNA adduct fluorescence is studied by following the emission spectra of the metal complexes of PAMTDA and PAETDA in the wavelength range of 530-700nm with an excitation wavelength of 520nm, upon addition of different metal complex concentrations to DNA pretreated with EtBr. The fluorescence quenching at around 590-610nm is described by the Stern-Volmer equation:

$I_o/I = 1 + K_{sv}r$ [44],

where I_o and I are the fluorescence intensities the DNA-EtBr adduct in the absence and the presence of complex respectively. K_{sv} is a linear Stern–Volmer quenching constant, r is the ratio of the total concentration of complex to that of DNA. Ksv values (M^{-1}) were obtained from the graph (Table 6) and they indicate the extent of interaction of the metal-complex with the DNA.

The emission spectra of DNA-EtBr (20 μM) in the absence and presence of increasing concentrations of the Zn(II) and Ni(II)complexes (20, 40, 60, 80 and 100 μM) of PAMTDA and PAETDA are shown in Fig. 18(a,b,c,&d). The arrow indicates the changes in the emission intensity as a function of complex concentration. It is generally agreed that strong fluorescence decrement accompanies a strong interaction of the metal complex with calf thymus DNA.

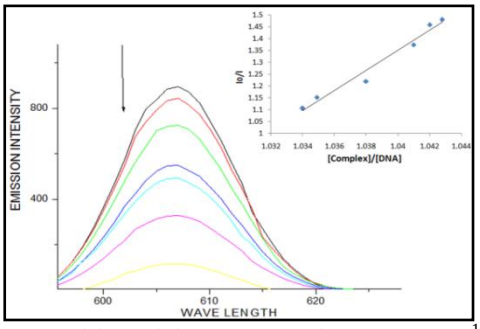

Fig.18(a): Zn(II)-PAMTDA (Ksv=0.279M^{-1})

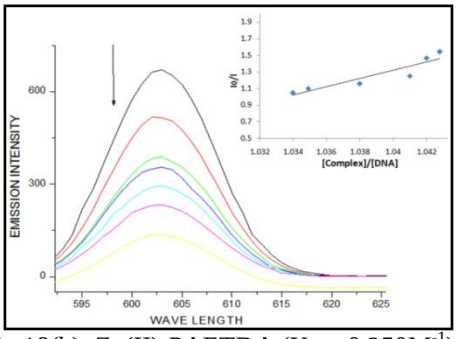

Fig.18(b): Zn(II)-PAETDA (Ksv=0.250M^{-1})

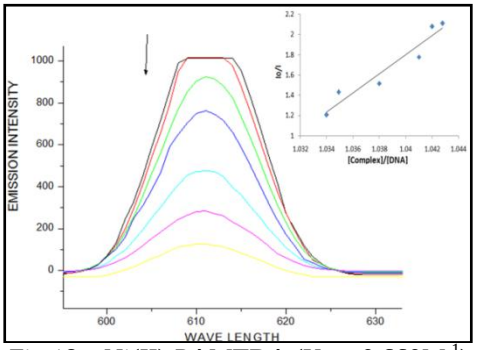

Fig.18c: Ni(II)-PAMTDA (Ksv=0.660M^{-1})

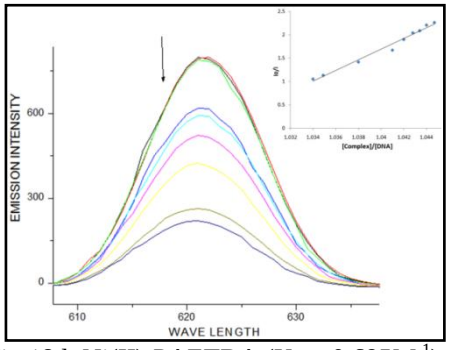

Fig.18d: Ni(II)-PAETDA (Ksv=0.695M^{-1})

(Insert: Stern-Volmer plot of the fluorescence titration data.)

Fig. (18a,18b,18c&18d) Emission spectra of Zn(II) and Ni(II) complexes showing fluorescence quenching on increasing the concentration of metal-complex.

Table: 6 Ksv Data of the complexes

Metal -Complex	Zn(II)-PAMTDA	Zn(II)-PAETDA	Ni(II)-PAMTDA	Ni(II)-PAETDA
Ksv values (M^{-1})	0.279	0.25	0.66	0.695

3.4.3**.** DNA viscosity measurements: DNA viscosity were carried out to support the results obtained from Electronic absorption and Fluorescence studies. Viscosity is strictly dependant on the change in length of DNA, an intercalative metal complex causes a separation of the base pairs, in order to get accommodated in the DNA structure, leading to a lengthening of the nucleic acid helix and an increase in its viscosity. DNA viscosity experiments are carried out in especially designed viscometers and the temperature is strictly controlled at 30^{o}C [45,46] using thermostatic bath.

From the data obtained a graph is drawn, $(\eta/\eta_0)^{1/3}$ *versus* the ratio of the compound to DNA concentration, where η is the viscosity of DNA in the presence of the metal complex and η_0 is the viscosity of the DNA alone. Viscosity values are calculated with the observed flow time of a DNA solution (t), corrected with the flow time of the buffer alone (t_0): $\eta = t - t_0 / t_0$**[**47].

The plots of relative viscosities showed significant change in the viscosity of DNA up on addition of metal complex and is comparable to the classical intercalator, ethidium bromide Fig. (19a &19b).

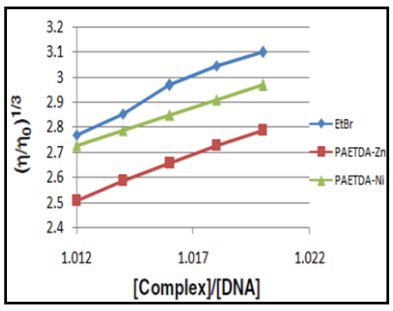

Fig19a: Zn(II) & Ni(II) complexes of PAMTDA

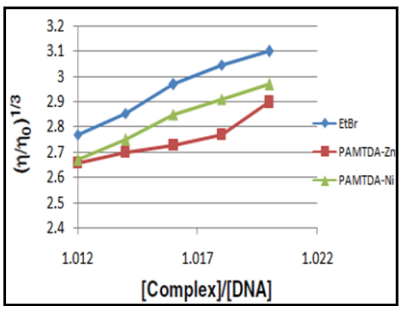

Fig19b: Zn(II) & Ni(II) complexes of PAETDA

Fig.19(a,b): Effect of increasing concentrations of EtBr(blue line), Zn(II)-PAMTDA, Zn(II)-PAETDA Complexes (redline), Ni(II)-PAMTDA, Ni(II)-PAETDA Complexes(green line) on the relative viscosity of CT-DNA.

3.5. Antimicrobial activity:

The ligands and their complexes were screened for antimicrobial activity and it was found that they possess anti bacterial activity against bacterial strains of Escherichia coli, Staphylococcus aureus, Bacillus substilis [gram(+ve)], Klebsiella pneumonia [gram(-ve)]. The compounds were tested at concentration 50µg/1ml of DMSO using Disc diffusion method using gentamycin as standard. The diameter of susceptibility zone was measured in mm. It was found that the diamagnetic Zn(II) complexes showed more activity against bacteria than the paramagnetic complexes and also more activity compared to ligands. (Table7).

Table 7: Anti Bacterial Activity of ligands and their complexes

SAMPLE	Staphylococcus aureus	Eischeria coli	Bacillus substilis	Klebsiella pneumonia
PAETDA	6 mm	8mm	-	-
Zn-PAETDA	27mm	21mm	25mm	16mm
Ni-PAETDA	-	10mm	-	-
PAMTDA	-	6mm	6mm	-
Zn-PAMTDA	-	22mm	27mm	-
Ni-PAMTDA	-	8mm	10mm	-

IV. Conclusions

The complexes obtained were characterized using various spectro-analytical techniques and the geometry of all the complexes proposed to be octahedral. From equilibrium studies, it was found that PAMTDA has less pK_a than PAETDA and all the metal complexes has 1:1 M-L ratio (Log β= $LogK_1$), where as for Ni-PAETDA has 1:2 M-L ratio(Log β= $LogK_1$+ Log K_2) . The stability of complexes follows the Irving William series of stability of metal complexes.

Energy parameters from computational calculations show possible coexistence of keto and enol forms. In Electrostatic potential, nitrogen atoms in thiadiazole ring and oxygen with amide linkage indicate negative ESP, hence more susceptible to electrophilic attack by a suitable agent. Energy gap between HOMO and LUMO proved stability and hardness of the molecule. QSAR properties generated show good penetrating capacity of the ligand into cell membrane.

DNA binding studies and anti microbial studies were also carried out and it was found that Ni(II)-PAETDA and Zn(II)-PAETDA have high binding constant values (K_b) than Ni(II)-PAMTDA and Zn(II)-PAMTDA which are in accordance with the Ksv values obtained from the fluorometric studies. Anti microbial studies reveals that Zn(II) complexes have very high activity compared to ligands and Ni(II) complexes. Thus in this paper, the effectiveness of the binding of new Ni(II) and Zn(II) complexes is being confirmed by means of hypochromism in the electronic spectral studies and change in intensity of emission in the case of emission spectral studies. Further it is also confirmed by the viscosity studies. This shows that the metal-complex interacts with DNA base pairs effectively by classical intercalative mode. Since the search for new therapeutic agents is a continuous struggle, in the context of the increasing incidence of drug resistance, the data provided above will be useful in designing new drugs.

Acknowledgements

The authors thank Department of Microbiology, UCS, Osmania University for antibacterial studies, Nizam college, Osmania University for providing UV spectrophotometer and spectro-fluorometer for DNA binding studies.

References

[1]. Abhishek Kumar Jain, Simant sharma, Ankur vaidya, Veerasamy Ravichandran and Ram Kishore Agarwal. Chem Biol Drug Des. 2013;81:557-576.
[2]. Nizam ud in, Bano Q., Tiwari N., Giri S., Ind. J. chem. 1992; 31 (B): 714-718.
[3]. Yurii SLYUKA., Chem.met.Alloys., 2014,7; 37-41.
[4]. Shadab miyan siddiqui, Attarsalahuddin,AmirAzam., Med. chem. Res. 2013; 22: 1305- 1312.
[5]. Yang Hu., Chem. Rev. 2014 ;114 (10): 5572-5610.
[6]. Kemal SANCAK, Yasemin UNVER, Mustafa ER., Turk. J. Chem. 2007; 31:125-134
[7]. Vivekananda D., Biradar B.H.M., Mruthyunjayaswamy., The Scientific world Journal 2013, vol 2013, Article ID 451629.
[8]. Tanveer Ahmed, Arvind Kumar Singh, Nupur Jaiswal, Deepika Singh., International research Journal of Pharmacy. 2012; 3(3).
[9]. Vasoya S.L., Paghdar D.J, Chovati P.t.,and Joshi H.S., J. Sci, Islamic Republic Iran. 2005; 16: 33-36.
[10]. Shao yu YANGPing, LISHI-Rong WANG Fa-Song, Huwei-Bing.,Chinese J.Struct.Chem. 2011;30(6): 848-852.
[11]. Kempegowda, Senthil Kumar G.P., Dev Prakash and Tamizmani T., *Der Pharma Chemica.* 2011; 3(2):330-341.
[12]. Mishra L., Said M.K., Itokawa H. and Takevo K., Bio org med. Chem. 1995; 3: 1241-45.

[13]. Quaraishi M.A.and Khan S., Indian Journal of Chemical technology.September 2005; 12:576-581.
[14]. BENTISS F., Traisnel M.,.Lagrenee M., Journal of applied electrochemistry. 2001; 31:41-48, 2001.
[15]. Hamdi M. Hassaneen, Omar A.Miqdad, Nada M.Abunada, Ahmed A.Fares., Natural Science. 2011;3(3): 199-207.
[16]. Xiao ke zhang Hang sun, xiao-Qing shen and Hong xing wang., Synthesis and Reactivity in Inorganic, Metal-Organic, and Nano-Metal Chemistry. 2007;37:661-664.
[17]. Funatsukuri, G. and Ueda, M. , Chem.Abstr. 1967; 66:44430f Pandey K.S, Kumar L.S, Revanasiddappa H.D, Vijay B,Jayalakshmi B., Indian journal Chem. 2011; 42B:206-210.
[18]. Kadirova Sh.A., Nuralieva G.A., Alieva M.A., Talipov M.A., Tilyakov and Parpiev,N.A., O'Zbekistan Kimyo Journali.2007; 13:712.
[19]. Kadirova Sh.A., Nuralieva G.A., Alieva M.A., Talipov M.A., Tilyakov and Parpiev N.A., Russian Journal of General Chemistry.,2005,75:1962-1964.
[20]. Wojahn, Hans; Wuckel, Hildebert., Archiv, der Pharmazie and Berichteder Deutschen Pharmazeutischen Gelleschaft. 1951; 284: 53-62.
[21]. Rajeev S., Kumar D., Bhoop S.,. Singh V.K and. Sharma R, *Research Journal of Chemical Sciences, 3(2),* 2013, 79-84.
[22]. Singh R., Kumar D., GOswami Y.C. and Sharma R., *Arabian Journal of Chemistry*, 2014, DOI:10.10ma 16/j.arabjc.2014.10.022.
[23]. Smith S. J. and Sutcliffe B. T., *Reviews in Computational Chemistry*, *70*, 1997, 271–316.
[24]. Cramer C.J., *Essentials of Computational Chemistry: Theories and Models* (NJ: John Wiley & Sons, 2002).
[25]. Graham Patrick, *An Introduction to Medicinal Chemistry* (5th edition, Oxford University Press, 2013).
[26]. Firas Abdullah Hussan., Int. J. of Reseach in Pharmacy and chemistry.2012; 2(1): 58-65.
[27]. William Kemp, 1986. " NMR in chemistry; A multinuciear introduction", Mc Millan Publications.
[28]. Irving H .M. and Rossotti H.S., J.Chem. Soc. 1954; 2904.
[29]. Irving H.M. and Rossotti H.S., Acta. Chem Scand.1956; 10:72.
[30]. Vogel.A.I., (1968) "AText Book of Quantitative Inorganic Analysis" 3rd Ed. Longman Elbs, London. P.264.
[31]. Nakamoto. K, 1970 Infrared spectra of inorganic and coordination compounds 2nd edition (New york ; wiley Interscience).
[32]. Daniels T,Wendlandt W .W. and Gallagher P.K; 1973 Thermal analysis.(New york ; wiley) Melnik M., Potocnak I., Macaskova L., Miklos D. and.Holloway C.E., Polyhedron. 1996; 15(13): 2159-21.
[33]. Lever A B P 1984 Inorganic electronic spectroscopy 2nd edn(Amsterdam;Elsevier).
[34]. Rai B.K., Kumar M., J.Indian Counc.Chem. 2003;20: 22.
[35]. Sakthilatha D. and Rajavel R., RJPBCS. 2013; 4(3): 1114.
[36]. Li D.D., Tian J., Gu W., Liu X., yan S., J.Inorg Biochem. 2010; 104: 171-179.
[37]. Zhou C.Y., Zhao J., Wu Y.B., Yin C.X., Yang P., J.Inorg. Biochem. 2007;101: 10-18.
[38]. Pasternack R.F., Gibbs E.J., Villafranca J., Bio chemistry. 1983;22(10): 2406-2414.
[39]. Sathyadevi P., Krishnamoorthy P., Jayanthi E., Butorac R.R., Cowley A.H., Dharmaraj N., Inorganica Chimica Acta, 2012;384: 83-96.
[40]. Strothkamp K.G, Strothkamp R.E., Fluorescence measurements of ethidium binding to DNA. J. Chem. Educ., 1994; 71(1): 77-79.
[41]. Kumar P., Gorai I., Santra M.K., Mondal B., Manna D., Dalton Trans., 2012; 41: 7573-7581.
[42]. Lakowicz J.R., Webber G., Quenching of fluorescence by oxygen. A probe for structural fluctuations in macromolecules, Biochemistry (1973) 4161.
[43]. García-Giménez J.L., Alzuet G., Gonzáles-Alvarez M., Liu-Gonzáles M., Castiñeiras A.,Borrás J., J. Inorg. Biochem., 2009; 103: 243-255. García-Giménez J.L., Gonzáles-Alvarez M., Liu-Gonzáles M., Macías B., Borrás J., Alzuet G . J. Inorg. Biochem., 2009; 103: 923-934.
[44]. Satyanarayana S., Dabrowiak J. C., Chaires J. B., Biochemistry, (1993), 32, 2573.